THE JOURNAL OF PHYSICAL CHEMISTRY C

Article

pubs.acs.org/JPCC

Chairlike and Boatlike Graphane: Active Photocatalytic Water Splitting Solar-to-Hydrogen Energy Conversion under UV Irradiation

A. H. Reshak*

New Technologies Research Centre, University of West Bohemia, Univerzitni 8, 306 14 Pilsen, Czech Republic

ABSTRACT: Graphene sheets are zero gap semiconductors with exceptional properties. The zero gap of graphene renders the construction of graphene-based photocatalysts very difficult. To enhance and/or modify these properties, hydrogenated graphene, which is called graphane, is proposed. This in turn enhances graphene with significantly promoted charge migration, up-shifted conduction band (CB) level, enhances the potential the of CB, increases the band gap that favors the enhancement of the photocatalytic performance. Here, we investigated the suitability of two configurations of graphane, namely, chairlike and boatlike graphane to be used as active photocatalysts under ultraviolet (UV) irradiation. The optical absorption level exhibited an obvious enhancement in the UV region. The absorption edge of chairlike (boatlike) graphane is located at λ = 364.6.1 (λ = 334.1) nm, and the corresponding optical band gap is about 3.4 eV (3.71) eV, which well-matched with the UV region and the sufficient negative CB potential for H^+/H_2 reduction. On the basis of these results, one can conclude that chairlike and boatlike graphane could satisfy all requirements to be an efficient photocatalyst.

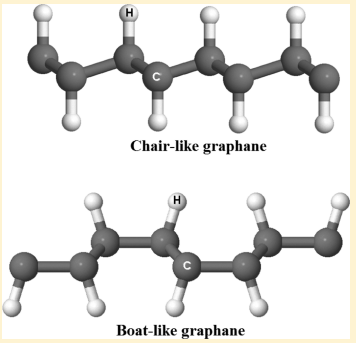

1. INTRODUCTION

After the discovery of graphene,[1,2] tremendous attention was focused on modifying newly discovered graphene; among them is the discovery of graphane.[3−10] Sluiter and Kawazoe[3] confirmed the existence of graphane and then after graphane was synthesized.[5] Since then, several new configurations for graphane were synthesized in several configurations (stirrup, boat-1, boat-2, twisted-boat, and chair). It has been reported that graphane has two favorable conformations: a chairlike conformer and boatlike conformer.[3,4,6,7,11−15] Graphane has potential applications as a hydrogen storage material. Xu et al.[16] reported that H_2O molecules are split into H_2 and $^{\bullet}OH$, which are then captured by the graphene surface under ultraviolet (UV) irradiation. Accordino et al.[17] have reported firm evidence for a neat hydrophilic nature of graphene surfaces.

In the current investigation, we focused on the comparison between the two favorable conformations: a chairlike conformer and boatlike conformer. Graphene, which is nontoxic and metal-free, shows huge capabilities for photocatalytic hydrogen evolution[18] and CO_2 reduction.[19,20] Graphene is nearly transparent to light and also a very good conductor of electricity; as a result, graphene could be used in combination with other photon-take devices to make the solar panels thin, flexible, and cheap. This could lead to a new generation of sun power echo-friendly energy. Nonetheless, the photocatalytic performance of graphene is restricted by its zero band gap. To remedy this drawback, various attempts have been made, such as exposing graphene sheets to hydrogen plasma (hydrogenated graphene).[5] The improvement in the performance of graphane is due to its high surface area that includes more active sites for reaction. The phenomenon of absorbing electromagnetic radiations is very important for a photocatalyst to be used for a clean environment and energy storage purpose. The high stability and reasonable band gap of graphane has been a fascinating research topic for theorists and experimentalists. This in turn enhances graphene with significantly promoted charge migration, up-shifted conduction band (CB) level, enhances the potential of the CB, and increases the band gap. We should emphasize that the layer structure favors the enhancement of the photocatalytic performance.[21]

The density function theory (DFT) is an efficient method to predict the material properties,[22−31] which has been used to explore new photocatalysts in excellent agreement with the experiment.[21,27−37] Therefore, we have used DFT to investigate the photocatalytic performance of chairlike and boatlike graphane as a novel, green, and an efficient photocatalyst. In our previous work, we calculated the linear optical and transport properties of the same materials.[38,39]

2. METHODOLOGY ASPECT

In this work, ab initio calculations were performed to study the photocatalytic performance of chairlike and boatlike graphane under UV irradiation. The chairlike conformer is stable in the $P\bar{3}m1$ space group, whereas the boatlike conformer is stable in the *Pmmn* space group.[3−5] The WIEN2k package[40] is used. The self-consistent calculations were achieved using the Perdew−Becke−Ernzerhof generalized gradient approximation (GGA-PBE),[41] and the ground state properties were obtained by using the Becke−Johnson (mBJ) potential scheme.[42] For the convergence of energy eigenvalues, the wave function in the interstitial regions were expended in plane waves with cutoff

Received: January 12, 2018
Revised: March 21, 2018
Published: April 3, 2018

DOI: 10.1021/acs.jpcc.8b00382
J. Phys. Chem. C XXXX, XXX, XXX−XXX

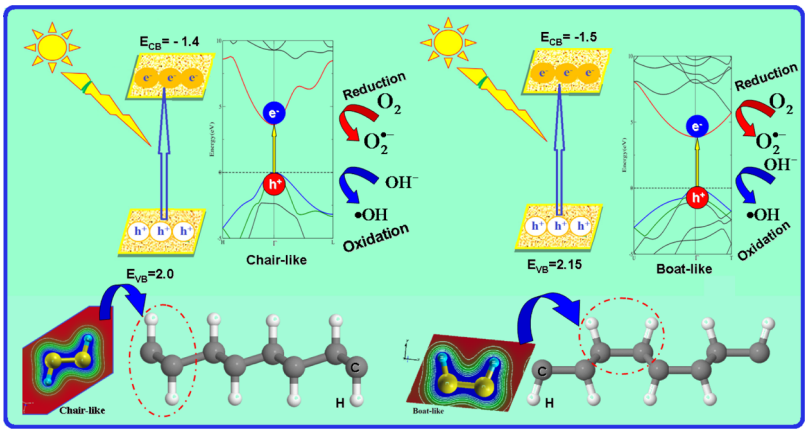

Figure 1. Schematic diagram of charge-transfer and photocatalytic mechanism of chairlike and boatlike graphane.

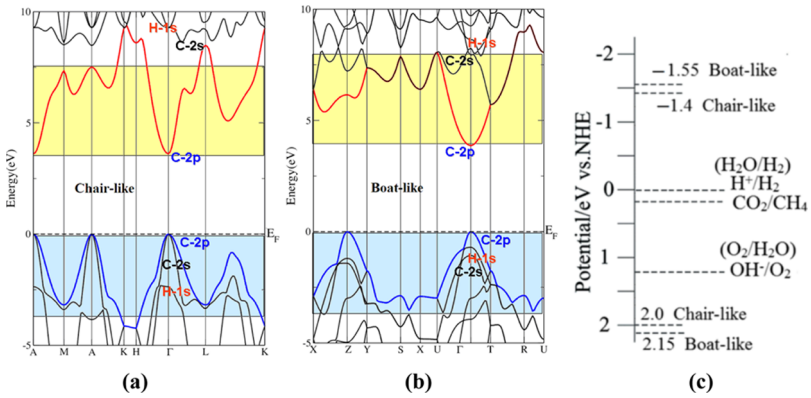

Figure 2. (a,b) Calculated electronic band structure of chairlike and boatlike graphane and (c) schematic diagram of potential in eV vs NHE for chairlike and boatlike graphane.

$R_{MT}K_{max}$ = 7.0, where R_{MT} and K_{max} stand for the muffin-tin (MT) sphere radius and magnitude of the largest K vector in plane-wave expansion, respectively. The chosen R_{MT} of a C atom is 1.43 (1.41) atomic units (au) for a chair (boat) conformer, whereas the R_{MT} of an H atom is 0.69 (0.68) au for a chair (boat) conformer. The wave function inside the sphere was expended up to l_{max} = 10, whereas the Fourier expansion of the charge density was up to G_{max} = 12 $(au)^{-1}$. The self-consistent calculations were converged with the difference in the total energy of the crystal and did not exceed 10^{-5} Ry for the successive steps. The self-consistent calculations were obtained by using 5000 k points in an irreducible Brillouin zone.

3. RESULTS AND DISCUSSION

The schematic diagram of charge-transfer and photocatalytic mechanism of chairlike and boatlike graphane is shown in Figure 1. Under illumination, the photocatalyst produces negative electron (e^-) and positive hole (h^+) pairs. Figure 1 illustrated that the photogenerated e^-−h^+ pairs are generated via band-to-band excitations; the photoexcited electrons are injected to the CB. Through proton (H^+)-aided multielectron processes for CO_2 photoreduction,[43,44] the photoexcited e^- can react with surface-adsorbed CO_2 in the existence of H^+ to evolve CH_4 as an elementary product. Meanwhile, the valence band (VB)-generated h^+ is involved in water oxidation, producing O_2 and H^+.[43,44]

Because the photocatalytic activities are associated with the electronic structure of the materials,[45] the electronic band structures of chairlike and boatlike graphane are presented in Figure 2a,b to explore the band dispersion, the orbitals that form the energy gap (E_g), and the nature of the fundamental E_g. It was found that both configurations possess a direct band gap because the CB minimum (CBM) and the VB maximum (VBM) are located along the A point (chairlike) and at Z point (boatlike), respectively. The obtained fundamental energy band gaps are about 3.67 eV (chairlike) and 3.98 eV (boatlike). A comparison of the obtained band gaps with those from earlier studies is presented in Table 1. It is interesting to highlight that the C 2p orbital plays a major role in the formation of the VBM, whereas the CBM is mainly formed by hybridized C 2p and C 2s. The VB is fashioned by hybridized C 2p, C 2s, and H 1s. One can also see strong hybridization between C 2s, C 2p, and H 1s states, favoring the enhancement of covalent bonding, as can be observed from electronic charge density contours. The covalent bonding is more favorable for the carrier transportation than the ionic one.[46] The C−C and C−H

Table 1. Calculated Energy Gap in Comparison to Previous Calculations

	chair-like	boat-like
LDA	2.69[a]	3.02[a]
GGA	3.02[a], 3.49[b], 3.5[c]	3.37[a], 3.37[b], 3.7[c]
EVGGA	3.60[a]	3.90[a]
mBJ (this work)	3.67	3.98

[a]Reference 38. [b]Reference 7. [c]Reference 4.

DOI: 10.1021/acs.jpcc.8b00382
J. Phys. Chem. C XXXX, XXX, XXX−XXX

bonds possess a strong electron cloud overlap that attracts h^+ and repels e^-, thus facilitating the separation of the e^-–h^+ pairs. This in turn enhances the photocatalytic performance.[47] The calculated C–C bond length is about 1.526 Å (1.554 Å) for chairlike (boatlike) graphane in good agreement with the previous work 1.52 Å (1.56 Å),[4] and the C–H bond length is about 1.135 Å (1.113 Å) for chairlike (boatlike) graphane in good agreement with the previous work 1.11 Å (1.10 Å).[4] Further, the H–C–C bond angle is calculated and it is found to be 107.81° (106.96°) for chairlike (boatlike) graphane.

It was noticed from Figure 2a,b that the bands around the Fermi level (E_F) possess low effective masses and hence high mobility carriers (Table 2), which favors the enhancement of the charge-transfer process. The higher photogenerated carrier mobility enhances the photocatalytic performance.[48,49] The large effective mass difference ($D = m_e^*/m_h^*$) between e^- and h^+ (Table 2) can expedite the e^- and h^+ migration and separation and enhance the photocatalytic performance. For chairlike graphane, the m_h^* is bigger than m_e^*, whereas for boatlike graphane, the m_h^* is lower than m_e^*, resulting in a significant mobility difference between e^- and h^+. The mobility of e^- and h^+ can be indirectly assessed by their m_e^* and m_h^* as follows: $((\text{mobility})_e = e\tau_e/m_e^*$ and $(\text{mobility})_h = e\tau_h/m_h^*)$. The large mobility difference is useful for the e^- and h^+ separation, reduction of the h^+ and e^- recombination rate, and improvement of the photocatalytic activity. Following Table 2, one can see that both m_h^* and m_e^* are small; therefore, one can conclude that the carrier transfer can be fast along different directions.

Table 2. Calculated Effective Masses

effective mass	chair-like	boat-like
m_e^*/m_o	0.010	0.018
m_{hh}^*/m_o	0.016	0.010
m_{lh}^*/m_o	0.006	0.020
$D = m_{hh}^*/m_e^*$	1.597	0.576
$D = m_e^*/m_{hh}^*$	0.625	1.733
$D = m_{lh}^*/m_e^*$	0.673	1.080
$D = m_e^*/m_{lh}^*$	1.485	0.925

The photocatalytic oxidation is mainly attributed to the participation of $O_2^{\bullet-}$, $^\bullet OH$, and h^+,[50] see Figure 1. To understand the photocatalytic mechanism of chairlike and boatlike graphane, the reduction potential of CBM and the oxidation potential of VBM at the point of zero charge can be estimated using the expressions:[51]

$$E_{CB} = \chi - E^C - (E_g/2) \quad (1)$$

$$E_{VB} = E_{CB} + E_g \quad (2)$$

The E_{CB} and E_{VB} values of chairlike and boatlike graphane are shown in Figure 2c. This figure illustrates the probable energy-level diagram [potential vs normal hydrogen electrode (NHE)] and CO_2 photoreduction, the relative positions of CBM and VBM for chairlike and boatlike conformers, and the redox potentials for CO_2/CH_4 and O_2/H_2O. Chairlike graphane appears to be a more efficient photocatalyst for CO_2 photoreduction, possessing a CBM at −1.40 eV and a corresponding VBM at 2.0 eV. The CBM lies above the redox potential of CO_2/CH_4 (0.17 eV), whereas the VBM lies above the O_2/H_2O redox potential (1.23 eV).[44] One can see that the

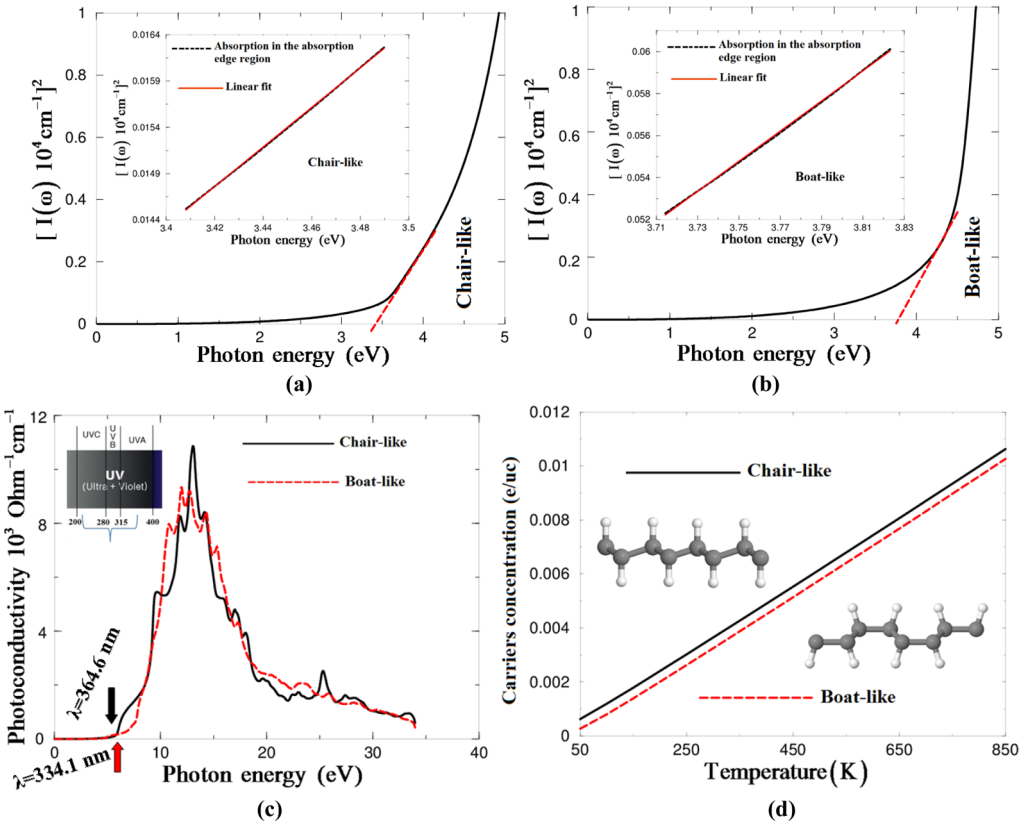

Figure 3. (a,b) Data plots of $[I(\omega)]^2$ vs photon energy in the absorption edge region; (c) photoconductivity of chairlike and boatlike graphane as a function of photon energy; and (d) carrier concentration of chairlike and boatlike graphane.

DOI: 10.1021/acs.jpcc.8b00382
J. Phys. Chem. C XXXX, XXX, XXX–XXX

CBM potential of boat-like graphane is much negative than that of chairlike graphane; therefore, boatlike graphane has a stronger reduction power for the production of H_2 than that of chairlike graphane.[51] The suitable E_g width and the appropriate CBM position together attribute to the optimal H_2 production activity. Thus, maintaining the equilibrium between the reduction power and the light absorption ability leads to a higher efficiency of light-driven photocatalytic H_2 production. Following Figure 2c, because of the higher CBM position, chairlike and boatlike graphane possess a large negative reduction potential of excited e^-, and thus, the CBM and VBM locations accommodate the redox capacity.

Because the free radicals $-OH$ and $-O_2^-$ possess a high oxidation number, they can oxidize various inorganic and organic C compounds to generate dioxide, H_2O, and other nontoxic small organic molecules. Thus, the E_g width defines the domain of the absorbed light (see Figure 3a,b). The absorption of the light induces the transfer of e^- from the VB → CB, creating e^-−h^+ pairs that can then migrate to the surface to contribute in oxidation and reduction reactions, respectively.[52,53] The positions of the CBM and the VBM defines the oxidation and reduction abilities of h^+ and e^-, respectively.[52,54] From the absorption spectrum (Figure 3a,b), the $E_{g(optical)}$ can be derived from $[I(\omega)]^2$ (the absorption coefficient). For the direct optical transitions, the $[I(\omega)]^2$ is linear with photon energy ($h\nu$) in the absorption edge region, whereas for indirect optical transitions, the $[I(\omega)]^{1/2}$ is linear with $h\nu$.[29] The inset of Figure 3a,b illustrates the graphs of $[I(\omega)]^2$ versus $h\nu$ in the absorption edge region for chairlike and boatlike conformers; one can see that the $[I(\omega)]^2$ versus $h\nu$ is linear in the absorption edge region; thus, the absorption edge of chairlike and boatlike conformers is caused by direct optical transitions. Figure 3a,b reveals that the absorption edge of chairlike and boatlike conformers occurs at λ = 364.6 nm (chairlike) and λ = 334.1 nm (boatlike), which correspond to the $E_{g(optical)}$ (λ_g = $1239.8/E_{g(optical)}$[55]) 3.40 eV (chairlike) and 3.71 eV (boatlike). That well-matched with UV irradiation and the sufficient negative CB potential for H^+/H_2 reduction. For more information, photoconductivity as a function of $h\nu$ is calculated and presented in Figure 3c. One can see that chairlike (boatlike) graphane shows the highest photoconductivity when the photons possess an energy of about 3.40 (3.71) eV. Thus, the photocurrent is produced at the absorption edge, that is, 3.40 (3.71) eV, which implies that chairlike (boatlike) graphane exhibits photocurrent response in the UV region. This indicates that chairlike (boat-like) graphane may have good photocatalytic performance and agrees well with the foregoing photocatalytic activity measurement. The other crucial issue to understand in the photocatalytic mechanism of the chairlike and boatlike graphane is the concentration of the carriers (n) and their mobility. Here, we studied the influence of temperature (T) on n at a certain value of chemical potential ($\mu = E_F$). Figure 3d reveals that the carrierconcentration of chairlike and boatlike graphane increases linearly with increasing T.

To investigate the charge-transfer and bonding nature, the electronic charge density distribution of chairlike and boatlike graphane, which is derived from the reliable converge wave function,[56,57] is calculated in different crystallographic planes (Figure 4). According to Pauling scale, the low electronegativity difference between C and H atoms points to an almost nonpolar covalent bond.[58] The maximum charge is accumulated around C and H atoms, as indicated by the blue color.

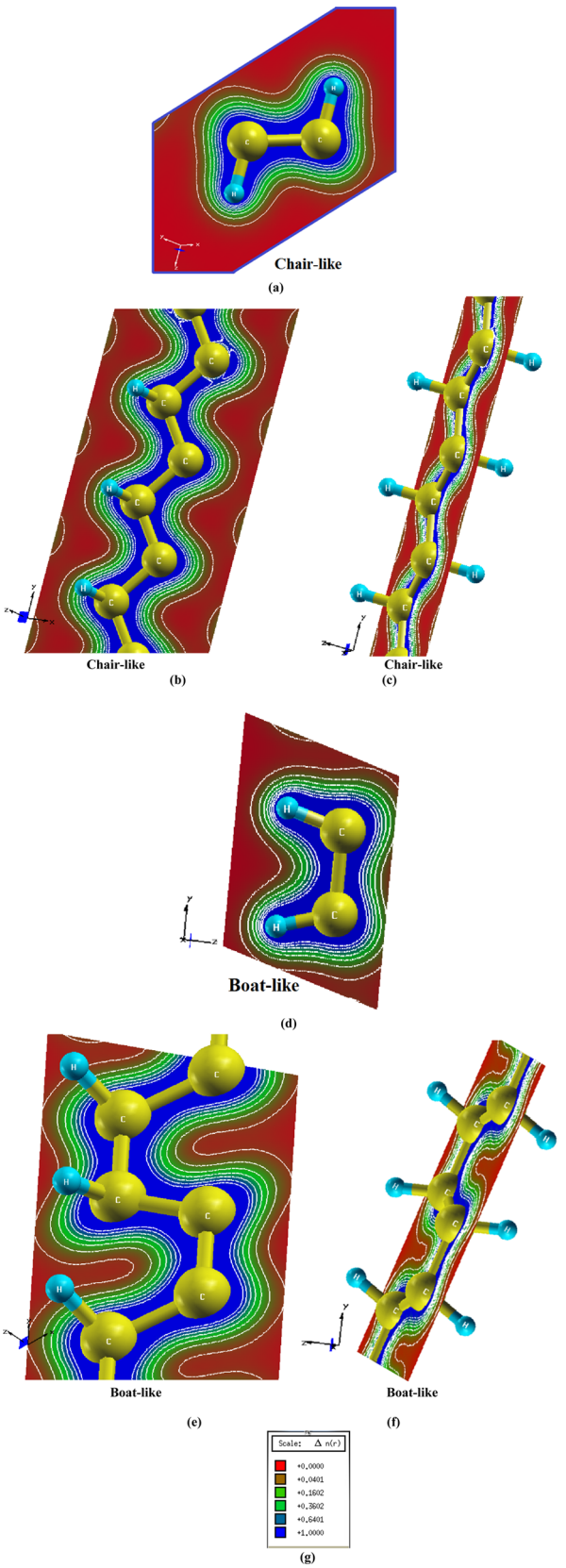

Figure 4. (a−f) Calculated electronic charge density distribution, which shows that C−C and C−H bonds possess a strong electron cloud overlap and prefer to attract holes and repel electrons, thus facilitating the separation of the photogenerated e^-−h^+ pairs. This in turn enhances the photocatalytic activity and (g) thermoscale.

DOI: 10.1021/acs.jpcc.8b00382
J. Phys. Chem. C XXXX, XXX, XXX−XXX

This implies that efficient charge transfer occurs toward the C atom due to the fact that the electronegativity of a C atom is larger than that of an H atom. The blue color refers to the maximum charge intensity (Figure 4g), which represents strong sharing of charge between C and H atoms resulting in a strong covalent bond. The red color represents zero charge (Figure 4g). Thus, the formation of chairlike and boatlike graphane efficaciously extends the local two-dimensional conjugated system of chairlike and boatlike graphane into a three-dimensional space and subsequently promotes the separation and mobility of charge carriers.

4. CONCLUSIONS

Hydrogenated graphene, which is called graphane is proposed to enhance graphene with significantly promoted charge migration, up-shifted CB level, enhance the potential of CB, increase the band gap as well as enhanced surface area that favors the enhancement of the photocatalytic performance. The chairlike and boatlike graphane are comprehensively investigated. The optical absorption edge moves from λ = 364.6.1 nm (chairlike) → λ = 334.1 nm (boatlike), which corresponds to the direct optical E_g of 3.4 eV (chairlike) → 3.71 eV (boatlike), that well-matched with UV irradiation and the sufficient negative CB potential for reduction of H^+/H_2. Chairlike graphane appears to be a more efficient photocatalyst for CO_2 photoreduction, possessing a CBM at −1.40 eV and a corresponding VBM at 2.0 eV. The CBM lies above the redox potential of CO_2/CH_4 (0.17 eV), whereas the VBM lies above the O_2/H_2O redox potential (1.23 eV). It can be clearly seen that for chairlike and boatlike graphane, the CB edge potential is less than the VB potential, indicating that chairlike and boatlike graphane has a strong reduction power for H_2 production. Generally, a suitable E_g value and an appropriate CBM location together attribute to the optimal H_2 production activity under light irradiation. Therefore, maintaining the equilibrium between the reduction power and the light absorption ability leads to a higher efficiency of light-driven photocatalytic H_2 production.

AUTHOR INFORMATION

Corresponding Author

*E-mail: maalidph@yahoo.co.uk.

ORCID

A. H. Reshak: 0000-0001-9426-8363

Notes

The author declares no competing financial interest.

ACKNOWLEDGMENTS

We would like to acknowledge the CENTEM project, CZ.1.05/2.1.00/03.0088, co-funded by the ERDF as part of the OP RDI program and CENTEM PLUS (LO1402).

REFERENCES

(1) Nakada, K.; Fujita, M.; Dresselhaus, G.; Dresselhaus, M. S. Edge state in graphene ribbons: Nanometer size effect and edge shape dependence. *Phys. Rev. B: Condens. Matter Mater. Phys.* **1996**, *54*, 17954.

(2) Okada, S. Energetics of nanoscale graphene ribbons: Edge geometries and electronic structures. *Phys. Rev. B: Condens. Matter Mater. Phys.* **2008**, *77*, No. 041408(R).

(3) Sluiter, M. H. F.; Kawazoe, Y. Cluster expansion method for adsorption: Application to hydrogen chemisorption on graphene. *Phys. Rev. B: Condens. Matter Mater. Phys.* **2003**, *68*, 085410.

(4) Sofo, J. O.; Chaudhari, A. S.; Barber, G. D. Graphane: A two-dimensional hydrocarbon. *Phys. Rev. B: Condens. Matter Mater. Phys.* **2007**, *75*, 153401.

(5) Elias, D. C.; Nair, R. R.; Mohiuddin, T. M. G.; Morozov, S. V.; Blake, P.; Halsall, M. P.; Ferrari, A. C.; Boukhvalov, D. W.; Katsnelson, M. I.; Geim, A. K.; Novoselov, K. S. Control of graphene's properties by reversible hydrogenation: evidence for graphane. *Science* **2009**, *323*, 610.

(6) Samarakoon, D. K.; Wang, X.-Q. Chair and Twist-Boat Membranes in Hydrogenated Graphene. *ACS Nano* **2009**, *3*, 4017.

(7) Leenaerts, O.; Peelaers, H.; Hernández-Nieves, A. D.; Partoens, B.; Peeters, F. M. First-principles investigation of graphene fluoride and graphane. *Phys. Rev. B: Condens. Matter Mater. Phys.* **2010**, *82*, 195436.

(8) Bhattacharya, A.; Bhattacharya, S.; Majumder, C.; Das, G. P. Transition-Metal Decoration Enhanced Room-Temperature Hydrogen Storage in a Defect-Modulated Graphene Sheet. *J. Phys. Chem. C* **2010**, *114*, 10297.

(9) Wen, X.-D.; Hand, L.; Labet, V.; Yang, T.; Hoffmann, R.; Ashcroft, N. W.; Oganov, A. R.; Lyakhov, A. O. Graphane sheets and crystals under pressure. *Proc. Natl. Acad. Sci. U.S.A.* **2011**, *108*, 6833.

(10) Samarakoon, D. K.; Chen, Z.; Nicolas, C.; Wang, X.-Q. Structural and electronic properties of fluorographene. *Small* **2011**, *7*, 965.

(11) Shkrebtii, A. I.; Heritage, E.; McNelles, P.; Cabellos, J. L.; Mendoza, B. S. Graphene and graphane functionalization with hydrogen: electronic and optical signatures. *Phys. Status Solidi C* **2012**, *9*, 1378−1383.

(12) Zhu, S.; Li, T. Hydrogenation-Assisted Graphene Origami and Its Application in Programmable Molecular Mass Uptake, Storage, and Release. *ACS Nano* **2014**, *8*, 2864−2872.

(13) Klimov, N. N.; Jung, S.; Zhu, S.; Li, T.; Wright, C. A.; Solares, S. D.; Newell, D. B.; Zhitenev, N. B.; Stroscio, J. A. Electromechanical properties of graphene drumheads. *Science* **2012**, *336*, 1557.

(14) Lee, C.; Wei, X.; Kysar, J. W.; Hone, J. Measurement of the Elastic Properties and Intrinsic Strength of Monolayer Graphene. *Science* **2008**, *321*, 385.

(15) He, C.; Zhang, C. X.; Sun, L. Z.; Jiao, N.; Zhang, K. W.; Zhong, J. Structure, stability and electronic properties of tricycle type graphane. *Phys. Status Solidi RRL* **2012**, *6*, 427−429.

(16) Xu, Z.; Ao, Z.; Chu, D.; Younis, A.; Li, C. M.; Li, S. Reversible Hydrophobic to Hydrophilic Transition in Graphene via Water Splitting Induced by UV Irradiation. *Sci. Rep.* **2014**, *4*, 6450.

(17) Accordino, S. R.; de Oca, J. M. M.; Fris, J. A. R.; Appignanesi, G. A. Hydrophilic behavior of graphene and graphene-based materials. *J. Chem. Phys.* **2015**, *143*, 154704. Leenaerts, O.; Partoens, B.; Peeters, F. M. Water on graphene: Hydrophobicity and dipole moment using density functional theory. *Phys. Rev. B: Condens. Matter Mater. Phys.* **2009**, *79*, 235440.

(18) Wang, X.; Maeda, K.; Thomas, A.; Takanabe, K.; Xin, G.; Carlsson, J. M.; Domen, K.; Antonietti, M. A metal-free polymeric photocatalyst for hydrogen production from water under visible light. *Nat. Mater.* **2009**, *8*, 76−80.

(19) Wang, X.; Chen, X.; Thomas, A.; Fu, X.; Antonietti, M. Metal-Containing Carbon Nitride Compounds: A New Functional Organic−Metal Hybrid Material. *Adv. Mater.* **2009**, *21*, 1609−1612.

(20) Mao, J.; Peng, T.; Zhang, X.; Li, K.; Ye, L.; Zan, L. Effect of graphitic carbon nitride microstructures on the activity and selectivity of photocatalytic CO_2 reduction under visible light. *Catal. Sci. Technol.* **2013**, *3*, 1253−1260.

(21) Reshak, A. H. Active Photocatalytic Water Splitting Solar-to-Hydrogen Energy Conversion: Chalcogenide Photocatalyst Ba_2ZnSe_3 under Visible Irradiation. *Appl. Catal., B* **2018**, *221*, 17−26.

(22) Atuchin, V. V.; Gavrilova, T. A.; Grivel, J.-C.; Kesler, V. G. Electronic structure of layered titanate Nd2Ti2O7. *Surf. Sci.* **2008**, *602*, 3095−3099.

(23) Atuchin, V. V.; Gavrilova, T. A.; Grivel, J.-C.; Kesler, V. G. Electronic structure of layered ferroelectric high-*k* titanate $La_2Ti_2O_7$. *J. Phys. D: Appl. Phys.* **2009**, *42*, 035305.

DOI: 10.1021/acs.jpcc.8b00382
J. Phys. Chem. C XXXX, XXX, XXX−XXX

(24) Khyzhun, O. Y.; Bekenev, V. L.; Atuchin, V. V.; Galashov, E. N.; Shlegel, V. N. Electronic properties of ZnWO4 based on ab initio FP-LAPW band-structure calculations and X-ray spectroscopy data. *Mater. Chem. Phys.* **2013**, *140*, 558−595.
(25) Huang, H.; Han, X.; Li, X.; Wang, S.; Chu, P. K.; Zhang, Y. Fabrication of Multiple Heterojunctions with Tunable Visible-Light-Active Photocatalytic Reactivity in BiOBr−BiOI Full-Range Composites Based on Microstructure Modulation and Band Structures. *ACS Appl. Mater. Interfaces* **2015**, *7*, 482−492.
(26) Huang, H.; Li, X.; Wang, J.; Dong, F.; Chu, P. K.; Zhang, T.; Zhang, Y. Anionic Group Self-Doping as a Promising Strategy: Band-Gap Engineering and Multi-Functional Applications of High-Performance CO_3^{2-}-Doped $Bi_2O_2CO_3$. *ACS Catal.* **2015**, *5*, 4094−4103.
(27) Huang, H.; He, Y.; Li, X.; Li, M.; Zeng, C.; Dong, F.; Du, X.; Zhangd, T.; Zhang, Y. $Bi_2O_2(OH)(NO_3)$ as a desirable $[Bi_2O_2]^{2+}$ layered photocatalyst: strong intrinsic polarity, rational band structure and {001} active facets co-beneficial for robust photooxidation capability. *J. Mater. Chem. A* **2015**, *3*, 24547−24556.
(28) Huang, H.; He, Y.; Lin, Z.; Kang, L.; Zhang, Y. Two Novel Bi-Based Borate Photocatalysts: Crystal Structure, Electronic Structure, Photoelectrochemical Properties, and Photocatalytic Activity under Simulated Solar Light Irradiation. *J. Phys. Chem. C* **2013**, *117*, 22986−22994.
(29) Zhang, J.; Yu, W.; Liu, J.; Liud, B. Illustration of high-active Ag_2CrO_4 photocatalyst from the first-principle calculation of electronic structures and carrier effective mass. *Appl. Surf. Sci.* **2015**, *358*, 457−462.
(30) Li, X.; Zhao, J.; Yang, J. Semihydrogenated BN Sheet: A Promising Visible-light Driven Photocatalyst for Water Splitting. *Sci. Rep.* **2013**, *3*, 1858.
(31) Hwang, D. W.; Lee, J. S.; Li, W.; Oh, S. H. Electronic Band Structure and Photocatalytic Activity of Ln2Ti2O7 (Ln = La, Pr, Nd). *J. Phys. Chem. B* **2003**, *107*, 4963−4970.
(32) Liu, C.; Zhang, Y.; Dong, F.; Reshak, A. H.; Ye, L.; Pinna, N.; Zeng, C.; Zhang, T.; Huang, H. Chlorine intercalation in graphitic carbon nitride for efficient photocatalysis. *Appl. Catal., B* **2017**, *203*, 465−474.
(33) Reshak, A. H. Photocatalytic water splitting solar-to-hydrogen energy conversion: Perovskite-type hydride XBeH3 (X = Li or Na) as active photocatalysts. *J. Catal.* **2017**, *351*, 119−129.
(34) Reshak, A. H. Photophysical, transport and structure properties of Tl10Hg3Cl16 single crystals: Novel photocatalytic water-splitting solar-to-hydrogen energy conversion. *J. Catal.* **2017**, *352*, 142−154.
(35) Reshak, A. H.; Auluck, S. Photocatalytic water-splitting solar-to-hydrogen energy conversion: Novel LiMoO3(IO3) molybdenyl iodate based on WO3-type sheets. *J. Catal.* **2017**, *351*, 1−9.
(36) Reshak, A. H. Quantum Dots in Photocatalytic Applications: Efficiently Enhancing Visible Light Photocatalytic Activity by integrating CdO quantum dots as sensitizer. *Phys. Chem. Chem. Phys.* **2017**, *19*, 24915.
(37) Huang, H.; Tu, S.; Zeng, C.; Zhang, T.; Reshak, A. H.; Zhang, Y. Macroscopic Polarization Enhancement Promoting Photo- and Piezoelectric-Induced Charge Separation and Molecular Oxygen Activation. *Angew. Chem., Int. Ed.* **2017**, *129*, 12022.
(38) Reshak, A. H.; Auluck, S. Electronic and Optical Properties of Chair-like and Boat-like Graphane. *RSC Adv.* **2014**, *4*, 37411.
(39) Reshak, A. H. Thermoelectric properties of fully hydrogenated graphene: Semi-classical Boltzmann theory. *J. Appl. Phys.* **2015**, *117*, 225104.
(40) Balaha, P.; Shewartz, K.; Madsen, G. K. H.; Kvsnicka, D.; Luitz, J. *WIEN2k, An Augmented Plane Wave + Local Orbitals Program for Calculating Crystals Properties*; Technische Universität: Wien, Austria, 2001; ISBN 3-9501031-1-2.
(41) Perdew, J. P.; Burke, S.; Ernzerhof, M. Generalized Gradient Approximation Made Simple. *Phys. Rev. Lett.* **1996**, *77*, 3865.
(42) Tran, F.; Blaha, P. Accurate Band Gaps of Semiconductors and Insulators with a Semilocal Exchange-Correlation Potential. *Phys. Rev. Lett.* **2009**, *102*, 226401.
(43) Xie, S.; Zhang, Q.; Liu, G.; Wang, Y. Photocatalytic and photoelectrocatalytic reduction of CO_2 using heterogeneous catalysts with controlled nanostructures. *Chem. Commun.* **2016**, *52*, 35−59.
(44) Chang, X.; Wang, T.; Gong, J. CO_2 photo-reduction: insights into CO_2 activation and reaction on surfaces of photocatalysts. *Energy Environ. Sci.* **2016**, *9*, 2177−2196.
(45) Zhou, P.; Wu, J.; Yu, W.; Zhao, G.; Fang, G.; Cao, S. Vectorial doping-promoting charge transfer in anatase TiO2 {0 0 1} surface. *Appl. Surf. Sci.* **2014**, *319*, 167−172.
(46) Wu, F.; Song, H.; Jia, J.; Hu, X. Effects of Ce, Y, and Sm doping on the thermoelectric properties ofBi2Te3 alloy. *Prog. Nat. Sci.: Mater. Int.* **2013**, *23*, 408−412.
(47) Fan, X.; Zang, L.; Zhang, M.; Qiu, H.; Wang, Z.; Yin, J.; Jia, H.; Pan, S.; Wang, C. A Bulk Boron-Based Photocatalyst for Efficient Dechlorination: K3B6O10Br. *Chem. Mater.* **2014**, *26*, 3169−3174.
(48) Tang, J.; Ye, J. Photocatalytic and photophysical properties of visible-light-driven photocatalyst $ZnBi_{12}O_{20}$. *Chem. Phys. Lett.* **2005**, *410*, 104−107.
(49) Sato, J.; Kobayashi, H.; Inoue, Y. Photocatalytic Activity for Water Decomposition of Indates with Octahedrally Coordinated d10 Configuration. II. Roles of Geometric and Electronic Structures. *J. Phys. Chem. B* **2003**, *107*, 7970−7975.
(50) Zhou, P.; Yu, G.; Jaroniec, M. All-Solid-State Z-Scheme Photocatalytic Systems. *Adv. Mater.* **2014**, *26*, 4920−4935.
(51) Li, Q.; Meng, H.; Zhou, P.; Zheng, Y.; Wang, J.; Yu, J.; Gong, J. Zn1−xCdxS Solid Solutions with Controlled Bandgap and Enhanced Visible-Light Photocatalytic H2-Production Activity. *ACS Catal.* **2013**, *3*, 882−889.
(52) Zhang, J.; Yu, W.; Liu, J.; Liu, B. Illustration of high-active Ag_2CrO_4 photocatalyst from the first-principle calculation of electronic structures and carrier effective mass. *Appl. Surf. Sci.* **2015**, *358*, 457−462.
(53) Wu, J.-C.; Zheng, J.; Wu, P.; Xu, R. Study of Native Defects and Transition-Metal (Mn, Fe, Co, and Ni) Doping in a Zinc-Blende CdS Photocatalyst by DFT and Hybrid DFT Calculations. *J. Phys. Chem. C* **2011**, *115*, 5675−5682.
(54) Banerjee, S.; Gopal, J.; Muraleedharan, P.; Tyagi, A. K.; Raj, B. Physics and chemistry of photocatalytic titanium dioxide: Visualization of bactericidal activity using atomic force microscopy. *Curr. Sci.* **2006**, *90*, 1378−1383.
(55) Carlsson, J. M.; Hellsing, B.; Domingos, H. S.; Bristowe, P. D. Theoretical investigation of the pure and Zn-doped α and δ phases of Bi2O3. *Phys. Rev. B: Condens. Matter Mater. Phys.* **2002**, *65*, 205122.
(56) Hoffmann, R. A chemical and theoretical way to look at bonding on surfaces. *Rev. Mod. Phys.* **1988**, *60*, 601.
(57) Gelatt, C. D.; Williams, A. R.; Moruzzi, V. L. Theory of bonding of transition metals to nontransition metals. *Phys. Rev. B: Condens. Matter Mater. Phys.* **1983**, *27*, 2005.
(58) Gao, F.; He, J.; Wu, E.; Liu, S.; Yu, D.; Li, D.; Zhang, S.; Tian, Y. Hardness of Covalent Crystals. *Phys. Rev. Lett.* **2003**, *91*, 015502.

DOI: 10.1021/acs.jpcc.8b00382
J. Phys. Chem. C XXXX, XXX, XXX−XXX